Available online at www.sciencedirect.com

ScienceDirect

Physics Procedia (2016) 000–000

Physics Procedia

www.elsevier.com/locate/procedia

9th International Conference on Photonic Technologies - LANE 2016

Yb-Fibre laser welding of 6 mm duplex stainless steel 2205

M. Bolut[a,b,*], C.Y. Kong[b], J. Blackburn[b], K.A. Cashell[a], P.R. Hobson[a]

[a]*Brunel University London, Kingston Lane, Uxbridge, UB8 3PH, United Kingdom*
[b]*TWI Ltd, Granta Park, Great Abington, Cambridge CB1 3QL, United Kingdom*

Abstract

Duplex stainless steel (DSS) is one of the materials of choice for structural and nuclear applications, having high strength and good corrosion resistance when compared with other grades of stainless steel. The welding process used to join these materials is critical as transformation of the microstructure during welding directly affects the material properties. High power laser welding has recently seen an increase in research interest as it offers both speed and flexibility. This paper presents an investigation into the important parameters affecting laser welding of DSS grade 2205, with particular focus given to the critical issue of phase transformation during welding. Bead-on-plate melt-run trials without filler material were performed on 6 mm thick plates using a 5 kW Yb-fibre laser. The laser beam was characterized and a Design of Experiment approach was used to quantify the impact of the process parameters. Optical metallographic methods were used to examine the resulting microstructures.

Peer-review under responsibility of the Bayerisches Laserzentrum GmbH.

Keywords: Fibre laser welding; duplex stainless steel; grade 2205

1. Introduction

Duplex stainless steels (DSS) are increasing in popularity owing to their outstanding material properties in terms of corrosion and strength. Grade 2205 (also certified to material grades UNS S31803, UNS S32205 and 1.4462) is the most commonly used grade of DSS in structural applications. By maintaining an equal proportion of ferrite and austenite phases, this material has high strength (yield strength of around 450 MPa) and excellent resistance to stress corrosion cracking (SCC) provided by the ferrite, as well as good ductility and general corrosion resistance provided

* Corresponding author. Tel.: +44-1223-8990-26 .
E-mail address: maxime.bolut@brunel.ac.uk

by the austenite. DSS can be found in bridges, marine structures and nuclear applications where the environmental conditions are harsh or long-term structural stability is required, International Molybdenum Association (2014). For instance, in the UK, grade 2205 is used for intermediate level nuclear waste containers.

The welding technique used in the manufacturing of these containers requires careful consideration. A number of studies (e.g. Svensson and Gretoft (1986), El-Batahgy (2011)) have reported that the microstructural changes during welding, as the material melts, have a profound impact on the structural performances. The ferrite–austenite transformation during welding, leading to the final phase balance, is dependent on the material composition and the cooling rate. Grade 2205 solidifies primarily in the fully ferritic phase and this is followed by the time-dependent formation of the austenite phase through solid-state transformation, Gunn (1997). Welds resulting in a low ferrite content (< 30 %) can reduce the resistance to SCC, whereas a high ferrite content (> 70 %) can reduce the toughness and the resistance to pitting corrosion. Within the range of 30 to 70 % of ferrite at the weld, these detrimental reductions in toughness, pitting resistance and SCC resistance are less significant, Walker & Gooch (1991).

In recent years, laser welding has been viewed as an attractive alternative to the more traditional arc welding for DSS, mainly because of its higher processing speed and its versatility for different processes (e.g. cutting, brazing, welding and soldering). Recent progress in fibre laser technology has made it possible to combine good beam quality and high energy stability, Quintino et al. (2007), producing welds with significantly lower heat input than other welding process such as Tungsten Inert Gas (TIG) welding. Other benefits include lower distortion, reduced heat affected zone (HAZ) and fewer weld defects. Therefore, consistent weld profiles with deep root penetration can be achieved, resulting in negligible weld porosity, Vollertsen and Thomy (2005). In addition, the low heat input during laser welding provides a further advantage for grade 2205 in that detrimental precipitation can be avoided, Amman (2010). The common industrial approach to laser weld grade 2205 uses an expensive filler material over alloyed with nickel (i.e. ER2209). The reason for using a filler material during laser welding is to prevent undercut, improve gap bridging and to maintain the phase balance of the material. However, it adds costs to the process, increases its complexity and reduces its flexibility.

This paper investigates the feasibility of laser welding of grade 2205 without using a filler material. A detailed experimental investigation of the relationship between the variable process parameters (i.e. power, welding speed, focus position, and shielding gas) and the resulting welds, profiles and microstructure for grade 2205 was performed.

2. Experimental programme

2.1. Approach

To examine the effect that focus position, power, welding speed, and shielding gas have on the phase balance at the weld a total of 35 tests were completed in the current study. As stated in section 1, maintaining the phase balance to ensure that ferrites remain at 30 – 70 % is critical for welded DSS in structural applications. The bead-on-plate (BOP) test procedure was carried out on grade 2205 plates with a thickness of 6 mm. Practical experience at TWI has shown that BOP melt-run can be used as a reasonable basis for the optimization of butt welding procedures. The aim of this work was to produce a full penetration weld (keyhole mode) with equal concentrations of the ferrite and austenite phases. A qualitative approach was used to determine the process parameters (i.e. power, welding speed, focus position) to achieve a full penetration weld. In addition, a Design of Experiment approach was used to quantify the impact of changes in different weld parameters on the microstructure. Design of Experiment is a useful tool for optimizing processes and has been extensively used in other fields, Weissman and Anderson (2015).

2.2. Material and equipment

The test materials consisted of DSS grade 2205 plates with dimensions of 200×150×6 mm. The chemical composition of the materials was analyzed and the results presented in Table 1 were in accordance with the material standard BS EN 10088-2:2014.

Table 1. Chemical composition % by mass of 6 mm thick grade 2205 plate, the balance is iron.

C	Si	Mn	P	S	Cr	Mo	Ni	Al	As	Co
0.019	0.27	1.83	0.019	<0.003	22.7	2.90	5.55	0.02	<0.01	0.04
Cu	**Nb**	**Sn**	**Ti**	**V**	**W**	**N**				
0.15	<0.01	<0.01	<0.01	0.05	<0.04	0.16				

The laser used in the experiments was an IPG high-brightness (model YLS-5000), multi-mode ytterbium-doped (Yb-fibre) continuous wave (CW) laser. It operated at a wavelength of 1070 ± 10 nm and with a maximum power output of 5 kW. The beam was delivered to the welding head through a fibre optic cable with a 150 µm core diameter (Ø). The laser welding head consisted of a collimating and a focusing unit which had lenses of 100 mm and 200 mm focal length (FL), respectively. This optical set up led to a theoretical spot size of 300 µm. Laser power at the sample face was measured using an Ophir power meter (model 10K-W-BB-45). The beam intensity distribution was measured with a Prometec beam profiler (model UF-100) and the caustic of the laser beam was characterized.

The temperature changes in the sample during welding were measured using a Lumasense infrared pyrometer (model IMPAC IPE 140). The temperature readings were taken at a fixed location (i.e. 50 mm from the start of the 150 mm long weld), at a distance of 300 mm away from the heat source. The sampling interval was 10 ms, which was the shortest available. Due to hardware limitations, the maximum temperature recorded was 1100 ˚C. The emissivity setting was set at 70 % for all tests.

2.3. Set up

The test arrangement consisted of a laser processing head which was mounted on a 3-axis gantry. The focusing lens was protected from potential damage caused by fumes and spatters using an air-knife and a semi-consumable infrared transparent cover slide between the lower surface of the focusing lens and the work-piece. The weld cap was shielded by a flow of nitrogen gas (purity of 99.9 %) through four 10 mm diameter stainless steel tubes, in a panpipe arrangement, at a rate of 10 ℓ/min each. The plate under bead was shielded at a rate of 10 ℓ/min, using an efflux channel insert in the base of the welding jig. Fig.1 depicts the set up.

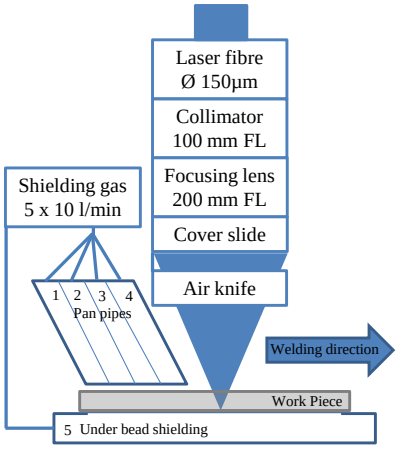

Fig. 1. Laser welding set up.

In a small number of trials, argon shielding gas was used for comparison. All BOP trials were performed autogenously in the flat (PA) position as covered by ISO 6947:2011. Immediately prior to laser welding, the material surfaces were cleaned using Scotch-Brite and then wiped using acetone.

Initial BOP trials were carried out using a welding speed from 0.5 to 5 m/min, laser power from 2.5 to 5 kW at focus position to achieved full penetration. This was followed by a designed set of experiments, generated using StatEase Design-Expert 8 software, to measure the impact of welding speed and focus position on the resulting

phase balance. A response surface methodology was used to generate the set of experiment, Myers et al. (2016), varying the welding speed from 0.8 to 2.2 m/min and focus position from +4 to -8 mm. Point counts, to determine the phase balance, of the resulting welds at the cap, middle and root location were fed back to the software as the responses.

2.4. Metallurgical assessment

The temperature of the weld surface was measured using the pyrometer and visually satisfactory samples were selected for metallography examination and x-ray radiography imaging to detect any potential internal defects. Selected samples were cross-sectioned, polished and then etched with a 40 % KOH (potassium hydroxide) solution for point count and 20 % H_2SO_4 (sulfuric acid) solution for cross section imaging. The point count method was carried out in accordance to ASTM E562:2002, by counting 32 fields with a 25 point grid at a magnification of one thousand. For point counting, the KOH etchant was preferable over sulfuric acid to give better contrast between the ferrite and austenite phases.

3. Results and discussion

3.1. Beam characterization

The laser power delivered to the work-piece was measured prior to welding trials to calibrate the system. The beam profile of the laser was also characterised. The beam radius was measured along the direction of light propagation (axis Z), giving the caustic show in Fig. 2 (a). From this data, the Rayleigh range Z_R was found to be 4.6 mm. Z_R describes the distance it takes, along Z axis, for the area of the cross section to be doubled and therefore gives a practical characterization of the beam divergence. The three-dimensional beam shape at focus is presented in Fig.2 (b).

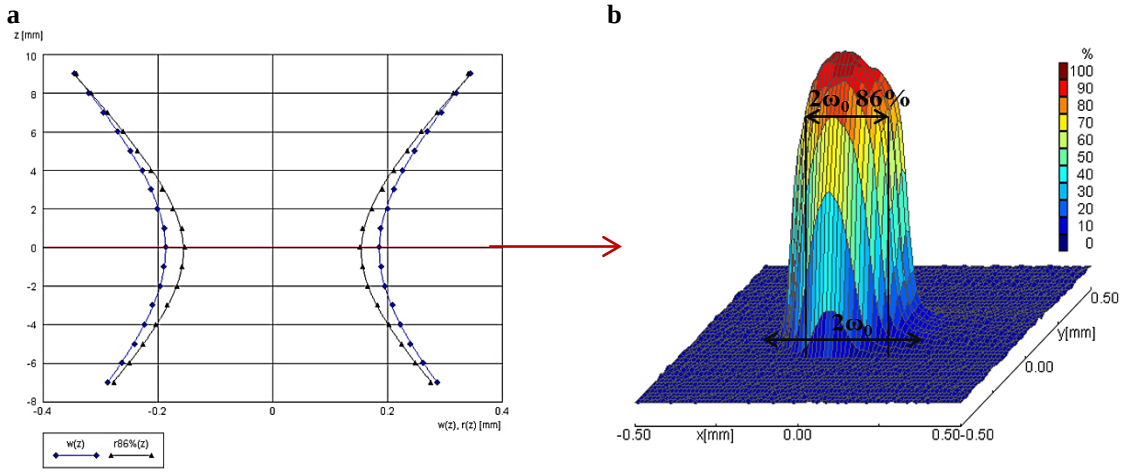

Fig. 2. (a) Caustic of the laser beam; (b) Beam shape at focus.

In Fig.2 (a) above, r86%(z) is the beam radius taking in account the $1/e^2$ definition i.e. the portion of the laser beam that contains 86 % of the total beam energy. Using this definition gives a beam diameter at focus position (i.e. 2 ω_0 86%) of 310 µm, very close from the theoretical value of 300 µm. The measured beam product parameter (BPP) was found to be 5.3 ± 0.5 mm. mrad which is compatible to the typical 5.5 mm. mrad given by the laser manufacturer.

3.2. Shielding gas

Shielding gases are necessary during welding to protect the melt pool from contamination and surface oxidation. Two different gases, nitrogen and argon, were used in these tests. Both resulted in clean welds which were free from oxidation, but argon shielded welds resulted in an average of 10 % higher ferrite content than welds produced in the same condition with nitrogen gas shielding. Similar work carried out previously on 3 mm thick grade 2205 showed similar differences. These results confirm that there is a significant advantage in using nitrogen shielding to promote austenite in the phase balance, in agreement with findings elsewhere, Keskitalo et al. (2015). Nitrogen shielding is believed to compensate for the losses of nitrogen in the melt pool caused by the welding process (e.g. plume, spatter). For this reason, nitrogen was used in subsequent work.

3.3. Process window for full penetration

As stated previously, the variables included in the tests were welding speed (0.5-5 m/min), power (3.5-5 kW). At focus position, the parameters required for full penetration are as follows:

- At 5 kW the maximum speed for full penetration was found to be below 4 m/min;
- A minimum of 4 kW of power is required with a welding speed of 1 to 2 m/min for full penetration; and
- At 0.5 m/min welding speed, the minimum power for full penetration was found to be above 2.5 kW.

3.4. Weld profile

No welding defects or porosity were observed following the radiograph and cross-section micrographs at 1000× magnification. Dimension measurements from BOP tests are summarized in Table 2 with Fig. 3 showing where they have been made. The standard BS EN ISO 13919-1:1997, which provides guidance on the quality levels for imperfections of steel welded with electron and laser beams, does not include information on the width of the weld cap or the weld root which is required for a good weld as weld dimensions are usually dependent on the particular application. However it was found that welding at speeds of 2 m/min or higher resulted in a narrower root of less than 1 mm in width, which was not desired for the welding of nuclear waste container. Weld cap were larger at slower welding speed varying from 3 to 2 mm in width and weld roots were in average 1 mm narrower.

Table 2. Weld profile measurements.

Parameters		**Dimensions (mm)**				
Welding speed (m/min)	Focus position (mm)	Cap	Excess metal cap	Waist	Root	Excess metal root
1	-4	3.3	0.32	1.24	1.94	0.05
1	-2	2.76	0.21	1.36	2.09	0.07
1	0	2.54	0.21	1.45	2.14	0.05
1.25	-4	2.59	0.18	1.12	1.25	0.06
1.25	-2	2.43	0.18	1.18	1.57	0.04
1.25	0	2.30	0.16	1.05	1.61	0.08
1.5	-4	2.56	0.12	1.00	1.29	0.17
1.5	-2	2.17	0.20	0.95	1.39	0.18
1.5	0	2.03	0.16	0.98	1.49	0.31
2	-6	2.37	0.24	0.76	0.67	0.33
2	-4	2.28	0.23	0.81	0.81	0.24
2.2	-2	1.92	0.3	0.67	0.69	0.32

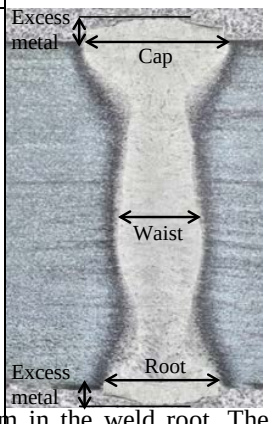

Fig. 3. Measurements sketch.

The maximum excess of metal was found to be 0.2 mm on the weld cap and 0.3 mm in the weld root. The standard BS EN ISO 13919-1:1997 allows up to 5 mm of weld excess for Level B (stringent) quality. Fig. 4 shows a

cross-sectioned micrograph of a full penetrating weld. The symmetrical weld about the axis of the laser beam suggests a steady fluid flow during welding and explains the absence of humping defects at the surface.

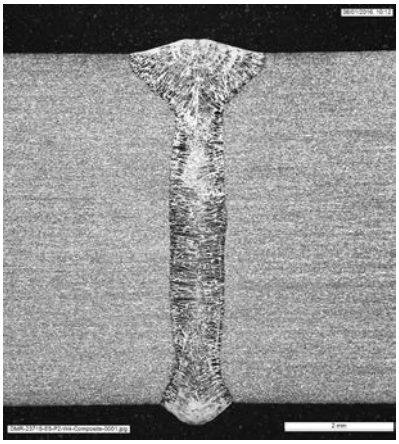

Fig. 4. Weld made at -2 focus at 4.5 kW with 1.5 m/min welding speed.

The focus position had an impact mostly on the weld cap width with a maximum difference of 0.8 mm observed between -4 focus and 0 focus at constant speed. Yet, the relatively low level of laser beam divergence compared with the material thickness limited the effect of the focus position (in the -4 to 0 mm range) on the waist and root width.

3.5. Temperature measurement

In these tests, the narrow high power laser beam, combined with a welding speed of 1 to 1.5 m/min, led to very low heat input (i.e. in the range of 0.2 to 0.3 kJ/mm compared to typical values of between 0.5 and 2.5 kJ/mm for the arc welding process). Fig. 5 shows the microstructure of the narrow HAZ for a typical sample at two magnification levels. A sharp transition in terms of crystal structure (shape and size) between the parent material and the weld was observed, suggesting a relatively fast cooling time due to the low heat input. It also suggests that there was a very contained heat flow at the weld location.

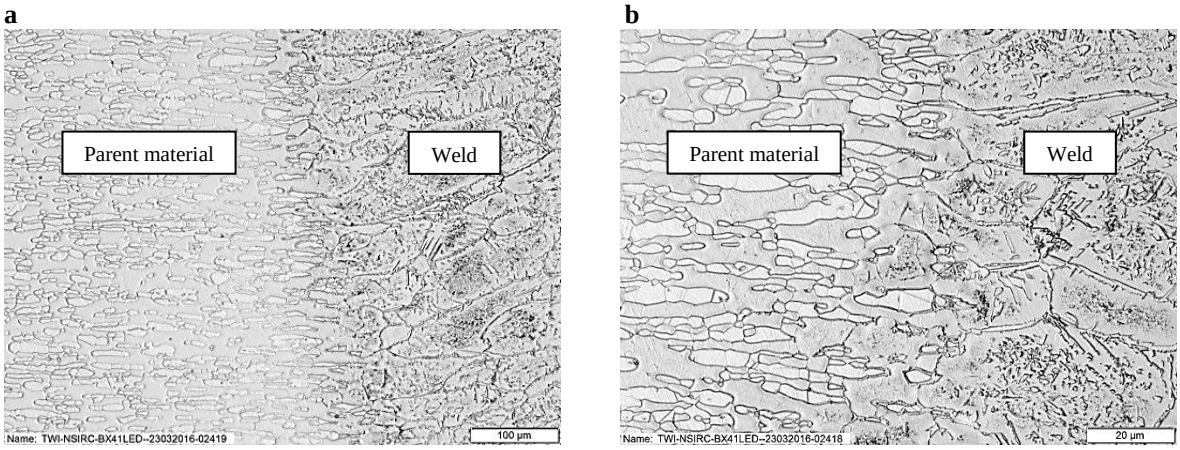

Fig. 5. (a) HAZ at 100 x magnification; (b) HAZ at 500 x magnification.

The changes in temperature at the weld cap were measured during the tests. Due to limitations in the equipment available, it was difficult to obtain absolute temperatures as the pyrometer operated with a single infra-red sensor,

which was unable to compensate for dynamic changes in emissivity between the liquidus and solidus phase. The pyrometer was nevertheless a useful tool for comparing qualitatively the effect of key parameters considered in this study. In all melt-runs, fast cooling rates exceeding 500 °C/s were measured and cooling rates approaching 1000 °C/s were observed when welding at 2 m/min speed. Decreasing the weld speed from 1.5 m/min to 1 m/min increases the cooling time, from 1100 to 800 °C, by 0.2 s. This extra time led to an average 5 % increase of austenite. Overall, the fast cooling rates hindered the austenite growth resulting in ferrite content exceeding the 70 % phase balance upper limit.

Fig. 6. Typical surface cool down of laser welded grade 2205 plot against isothermal precipitation.

Fig. 6 shows the time-temperature-transformation diagram of grade 2205, showing the typical temperature profile, measured during laser welding performed in this study. The fast cooling prevents the detrimental precipitation of chi, sigma, and carbide phases, Gunn (1997). As the typical cool down of the weld surface is significantly less than the time required for precipitations to occur, there is scope for improvement in the parameters. For example, using a higher laser power, slower welding speed or using beam shaping techniques. A slower cooling of the weld would allow more time for ferrite to transform into austenite to achieve the phase balance.

3.6. Phase transformation during laser welding

Microstructures of welds were examined using the optical metallographic method. Fig. 7 (a) and (b) show phases present in the parent material prior to welding and at the weld cap after welding.

a **b**

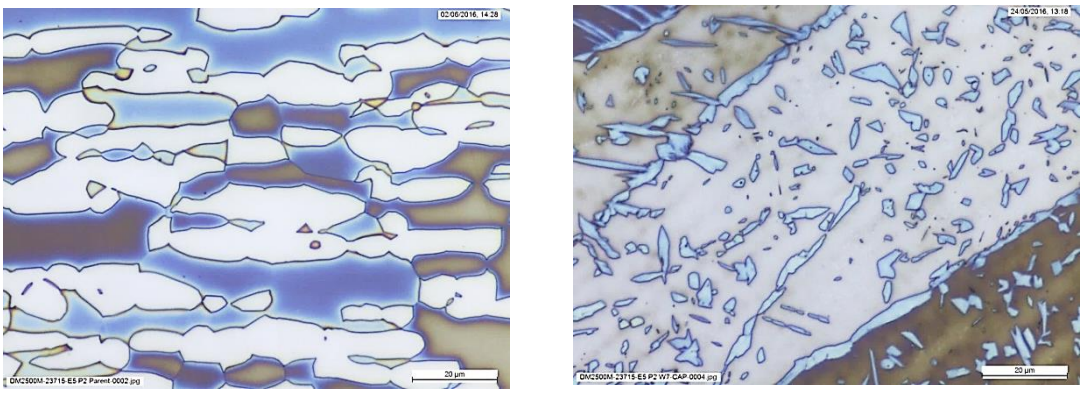

Fig. 7. Microstructure observation at 1000 x magnification at (a) base metal and (b) weld cap.

In order to assess the effect of the two process parameters (i.e. welding speed and focus position) on the resulting phase balance, the Design-Expert software was used to generate a designed set of experiments. Table 3 presents the test results including the percentage of ferrite at three locations - weld cap, waist and weld root. For each weld, manual

point counts of the ferrite content at these three locations were entered into the Design-Expert software as 'response'. A linear regression model was found to best fit the experimental ferrite content results with a 0.01 % chance that the model can occur due to noise.

Table 3. Design of Experiment: Process parameters and ferrite content.

Process parameters		**Ferrite content (%)**				
Welding Speed (m/min)	Focus position (mm)	Cap	Waist	Root	Average ferrite at the 3 locations	Standard deviation
0.8	-2	66.6	69.6	66.9	67.7	1.4
1	-6	67.9	75	73.6	72.2	3.1
1	2	67.4	69.8	72.2	69.8	2.0
1.5	-8	77.8	77.7	75.4	77.0	1.1
1.5	-2	75.4	81.6	67.1	74.7	5.9
1.5	-2	76.3	83.1	78.4	79.3	2.8
1.5	-2	79.4	84	76.8	80.1	3.0
1.5	4	73.8	84.8	86.1	81.6	5.5
2	-6	81.1	86.2	82.1	83.1	2.2
2	2	80.1	88.9	76.1	81.7	5.4
2.2	-2	82.1	85.1	74.3	80.5	4.6

An analysis of the variance (i.e. ANOVA analysis) gave for each process parameter the value of "Prob<F". A value less than 0.05 indicates that the process parameter is significant while a value greater than 0.1 is considered to be negligible. It was found for each response (ferrite content at the cap, waist and root) that:

- The focus position is an insignificant factor ("Prob<F">0.33).
- The welding speed is a significant factor ("Prob<F"<0.0001).

The welding speed and ferrite content are linearly correlated with high welding speed leading to high ferrite content. Fig. 8 shows the regression model with the error interval (shown as the dotted lines) of welding speeds and the resulting ferrite content. This correlation is due to the decreasing heat input and therefore faster cooling rate as the welding speed increases.

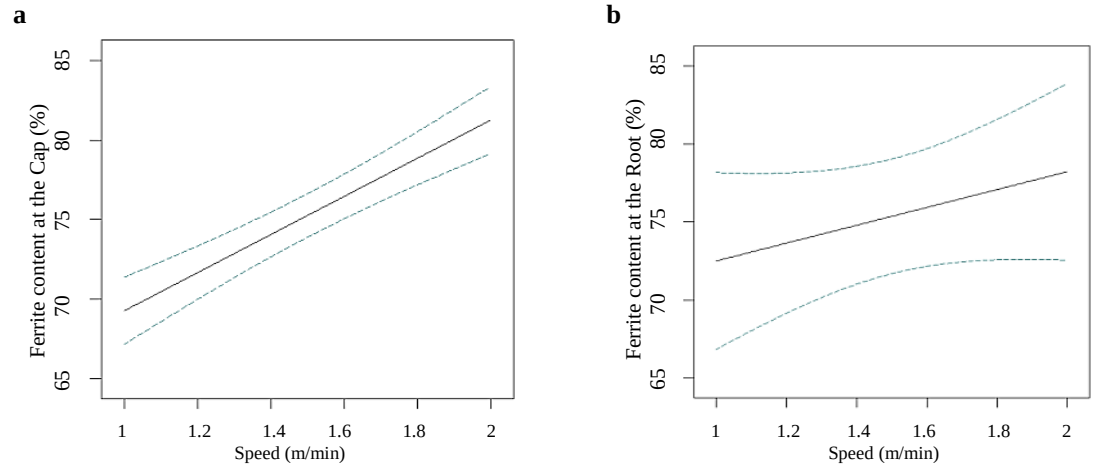

Fig. 8. (a) Predicted ferrite content for weld cap; (b) Predicted ferrite content for weld root.

The ferrite content was found to be high, exceeding the upper limit of 70 % in most cases. The process window predicted for achieving ferrite content below 70 % at the cap, middle and root is independent of the focus position (from -8 to +4 mm) but required to a welding speed below 0.5 m/min to increase the heat input.

4. Conclusions

This paper described a series of laser beam welding tests on DSS grade 2205 with a thickness of 6 mm. The process parameters studied were power, weld speed, choice of shielding gas and focus position. These were varied in order to understand their influence on the weld quality. The main conclusions from this study are summarized below:

- Grade 2205 was found to have a good weldability using a fibre laser. There were no visible cracks, porosity or other weld defects observed using x-ray radiography and optical microscope up to 1000 × magnification.
- As a result of the low divergence of the laser beam compared to the thickness of the material (Rayleigh range of 4.6 mm) it was found that the focus position had a negligible impact on the phase content.
- In comparison with argon shielding, using nitrogen gas was found to promote the growth of austenite phase by 10 % on average.
- Increasing the heat input by reducing the welding speed from 1.5 to 1 m/min extended the cool down at the material surface by 0.2 s. This lead to an increase of around 5 % austenite at the weld location.
- The process parameters considered in this study were unable to produce welds that contained ferrite phase less than the upper acceptable limit of 70 %. Higher heat input (e.g. using slower welding speeds) would be required to extend the cooling time in order to achieve higher austenite content in the weld. A welding speed of less than 1 m/min however is not preferred for the intended application (nuclear waste container manufacturing).

5. Further work

The work described in this paper is part of an ongoing test programme. Further work is necessary to investigate alternative, non-conventional welding approaches to achieve phase balance without filler. Work including beam shaping and multiple beam configurations is currently ongoing.

Acknowledgements

The author would like to acknowledge TWI Ltd and NSIRC for the equipment used and Graham Engineering Ltd for supplying the DSS samples used in this work.

References

Amman, T., 2010. Gas-shielded Arc Welding of ferrite-austenitic steels, Welding International, 24(11), pp.861-866.

El-Batahgy, A.-M., 2011. Effect of Laser Beam Welding Parameters on Microstructure and Properties of Duplex Stainless Steel. Materials Sciences and Applications, 02(10), pp.1443–1451.

International Molybdenum Association (IMOA), 2014. Practical Guidelines for the Fabrication of Duplex Stainless Steels 3rd ed., London, UK .

Keskitalo, M., Mäntyjärvi, K., Sundqvist, J., Powell, J., Kaplan, A.F.H., 2015. Laser welding of duplex stainless steel with nitrogen as shielding gas. Journal of Materials Processing Tech., 216, pp.381–384.

Myers, R.H., Montgomery, D.C. & Anderson-Cook, C.M., 2016. Response Surface Methodology: Process and Product Optimization Using Designed Experiments 4th ed., Wiley.

Gunn, R.N., 1997. Duplex Stainless Steels - Microstructure, properties and applications, Abington Publishing.

Quintino, L., Costa, A., Miranda, R., Yapp, D., Kumar, V., Kong, C.J., 2007. Welding with high power fiber lasers – A preliminary study. Material and Design, 28, pp.1231–1237.

Svensson, L.F. and Gretoft, B., 1986. Properties-Microstructure Relationship for Duplex Stainless Steel Weld Metals. In Proceedings of International Conference, Duplex Stainless Steel. Hague, paper 22.

Vollertsen, F. and Thomy, C., 2005. Welding with Fiber Lasers From 200 To 17000 W. ICALEO. paper 506.

Walker, R.A. and Gooch, T.G., 1991. Pitting Resistance of Weld Metal for 22Cr-5Ni Ferritic-Austenitic Stainless Steels. British Corrosion Journal, 26(1), pp.51–59.

Weissman, S. & Anderson, N.G., 2015. Design of Experiments (DoE) and Process Optimization. A Review of Recent Publications. Organic Process Research & Development, 19 (11), pp.1605–1633.